# Itinerant antiferromagnetism in $FeMnP_{0.8}Si_{0.2}$ single crystals

B. C. Sales,[1] M. A. Susner,[1] B. S. Conner,[1] J. Q. Yan,[1,2] and A. F. May[1]
[1]*Materials Science and Technology Division, Oak Ridge National Laboratory, Oak Ridge, Tennessee 37831, USA*
[2]*Department of Materials Science and Engineering, University of Tennessee, Knoxville, Tennessee 37996, USA*
(Received 1 July 2015; published 25 September 2015)

Compounds based on the $Fe_2P$ structure have continued to attract interest because of the interplay between itinerant and localized magnetism in a noncentrosymmetric crystal structure, and because of the recent developments of these materials for magnetocaloric applications. Here we report the growth and characterization of millimeter-sized single crystals of $FeMnP_{0.8}Si_{0.2}$ with the $Fe_2P$ structure. Single-crystal x-ray diffraction, magnetization, resistivity, and Hall and heat capacity data are reported. The crystals exhibit itinerant antiferromagnetic order below 158 K with no hint of ferromagnetic behavior in the magnetization curves and with the spins ordered primarily in the *ab* plane. The room-temperature resistivity is close to the Ioffe-Regel limit for a metal. Single-crystal x-ray diffraction indicates a strong preference for Mn to occupy the larger pyramidal $3g$ site. The cation site preference in the as-grown crystals and the antiferromagnetism are not changed after high-temperature anneals and a rapid quench to room temperature.

DOI: 10.1103/PhysRevB.92.104429 PACS number(s): 75.30.−m, 75.30.Sg, 75.50.Ee

## I. INTRODUCTION

The magnetic properties of hexagonal $Fe_2P$ and related alloys have been heavily investigated for over 40 years [1–7] and are intriguing because the observed behaviors have been described by the itinerant magnetism model of Moriya [8]. The $Fe_2P$ structure ($P\bar{6}2m$) has two distinct metal sites, $Fe_I$ and $Fe_{II}$. The smaller tetrahedral $Fe_I$ site ($3f$) has four P neighbors and the larger pyramidal $Fe_{II}$ site ($3g$) is coordinated by five P atoms. The pure compound exhibits a first-order ferromagnetic transition below 210 K with magnetic moments on the $Fe_I$ and $Fe_{II}$ sites of 0.92 and 1.70 $\mu_B$, respectively [9]. The magnetism of $Fe_2P$ is extremely sensitive to pressure [10] and small concentrations of chemical dopants such as Mn, Si, and B [3,11,12] can completely suppress ferromagnetism [3,10] or even triple the Curie temperature [11,12]! The large difference between the two iron moments in $Fe_2P$ suggests a mixture of itinerant and more localized magnetism, which is even more evident in Mn-doped alloys [13]. The recent interest in these compounds arises from two directions. First, the $Fe_2P$ crystal structure lacks inversion symmetry and these materials may exhibit complex, canted spin structures that can be manipulated with a magnetic field or an electrical current [14,15]. The complex spin structures are due to the effects of spin-orbit coupling as parameterized by the Dzyaloshinskii-Moriya (DM) interaction [16,17]. Second, various alloy compositions $(Fe,Mn)_2(P,As,Si,B)$ with the $Fe_2P$ structure show great promise as magnetocaloric materials for refrigeration [13,18–21]. Because of the extreme sensitivity of these materials to relatively small changes in composition [21] and the difficultly in preparing single-phase polycrystalline samples, the reported properties of many of these materials vary significantly due to the presence of impurity phases, up to 15% [22]. While some of these polycrystalline materials may be suitable for magnetocaloric applications, obtaining a fundamental microscopic understanding of the magnetism and the magnetoelastic coupling becomes difficult without high-purity single-crystal samples. This provided the motivation for the present study. Although there have been a few single-crystal investigations of the $Fe_2P$ type materials [1–3,6], in our study we have prepared single crystals with compositions similar to those proposed for magnetocaloric applications [13,20].

## II. SYNTHESIS AND EXPERIMENTAL METHODS

Single crystals of $Fe_{2-x}Mn_xP_{1-y}Si_y$ are grown out of a molten Sn flux. High-purity Fe and Mn pieces (Alfa Aesar, 99.98%), P chunks (Alfa Aesar, 99.999%), freshly ground Si powder (Alfa Aesar, 99.999%), and Sn shot (Alfa Aesar, 99.999%) are loaded into a 10-$cm^3$ alumina crucible in a typical molar ratio Fe:Mn:P:Si:Sn of 2:2:1:1:30. The alumina crucible containing all of the elements and a second "catch" crucible with quartz wool are sealed inside an evacuated silica tube. The mixture is heated to 1125°C held for 24 h and then cooled to 900 °C at 1.5 °C/h. The ampoule is then removed from the furnace and the excess molten Sn is centrifuged into the catch crucible. In most cases small needlelike crystals with the $Fe_2P$ structure weighing a few micrograms are obtained. These crystals are suitable for magnetization measurements and a few other experiments [23] but are too small for electrical transport and heat capacity measurements. The Fe to Mn ratio in the crystals could be controlled and is close to the starting ratio as long as the Fe/Mn ratio is between 1 and 1.8. For Fe/Mn values much less than 1, $Mn_2P$ crystals tend to grow, while for Fe/Mn values larger than 1.8, $Fe_5Si_3$ crystals dominate. The P/Si ratio is more difficult to control, and the maximum amount of Si in crystals with the hexagonal $Fe_2P$ phase is close to 0.3 (i.e., $P_{0.7}Si_{0.3}$) for the Fe/Mn ratios near 1.8, and about 0.2 for Fe/Mn ratios near 1. The limited control of the Si concentration in this type of growth is likely related to the smaller solubility of Si in molten Sn relative to the other elements [24]. For compositions near $FeMnP_{0.8}Si_{0.2}$ substantially larger crystals weighing a few milligrams are obtained [Fig. 1(c)]. These larger crystals frequently have Sn inclusions and sometimes a Sn core running along the length of the crystal which had to be ground away before measurements. This is extremely important for electrical measurements because of the high electrical conductivity of Sn relative to $FeMnP_{0.8}Si_{0.2}$ and the

 

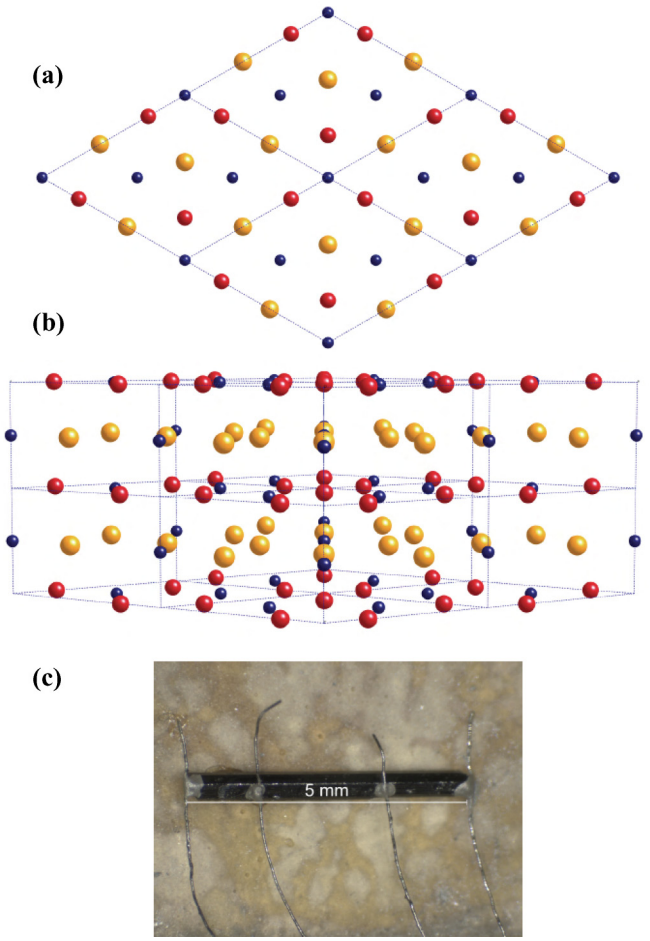


FIG. 1. (Color online) Crystal structure of $FeMnP_{0.8}Si_{0.2}$. View along the (001) direction (a), and view along (110) direction (b) The small P (Si) atoms are blue, the medium Fe atoms are red, and the largest Mn atoms are yellow. The structure is drawn with Mn fully occupying the pyramidal ($3g$) site and Fe the ($3f$) tetrahedral site, consistent with the single-crystal refinement results shown in Table I. For this ordered arrangment of Mn and Fe, the structure consists of alternating Fe and Mn layers, as shown in (b). (c) A 5-mm-long single crystal of $FeMnP_{0.8}Si_{0.2}$ with electrical leads attached.

giant magnetoresistance of Sn at low temperatures [25]. For the resistivity and Hall measurements, the crystals are polished to a 45-micron-thick plate. Electrical leads are attached to the crystals using 0.05-mm Pt wires and Epo-Tek H20E silver epoxy. The Hall data are taken using the standard four-point geometry [26] at fixed temperatures and with $H$ varying from $-6$ to $+6$ T in 1-T steps. The Hall resistivity, $\rho_H$, is obtained from the odd-in-$H$ part of the transverse resistivity $\rho_H = [\rho_{xy}(H) - \rho_{xy}(-H)]/2$. The chemical compositions of the crystals are determined using a Hitachi 3000 Tabletop scanning electron microscope with a Bruker Quantax 70 energy dispersive x-ray spectroscopy (EDS) system. The composition of all of the mm-sized crystals from a growth are the same within the resolution of the EDS system : $Fe_{1\pm0.02}Mn_{1\pm0.02}P_{0.8\pm0.02}Si_{0.2\pm0.01}$ From EDS measurements there is no evidence of Sn incorporation into the $Fe_2P$ structure or evidence of any composition variation along the length of the crystal.

Single-crystal x-ray diffraction patterns are collected on a Rigaku single-crystal diffractometer using Mo $K\alpha$ radiation. Each single-crystal diffraction experiment utilized $\sim$150 unique peak reflections for refinements to determine crystal structure. The site occupancies for the P/Si sites were determined at 230 K; these values were then used for the 110 K refinement. Magnetic data are collected using a Magnetic Property Measurement System from Quantum Design (QD). Heat capacity, resistivity, and Hall data are collected using a QD Physical Property Measuring System.

## III. RESULTS AND DISCUSSION

The structure of $FeMnP_{0.8}Si_{0.2}$ is shown is Fig. 1, along with a photograph of a crystal. From the single-crystal structure refinement, the $R1$ factors are smallest with Mn fully occupying the larger pyramidal $3g$ site and Fe the tetrahedral $3f$ site. The refinements are either unstable or yield an increase in the $R1$ factor if the metal sites are switched or randomized. No site preference for Si and P are evident in the refinements using the same technique. If the Mn and Fe sites are completely ordered, as indicated by the aforementioned results, the structure can be regarded as layered with alternating Mn and Fe layers stacked along the $c$ axis [Fig. 1(b)]. The structure is refined above (230 K), and below (110 K) the antiferromagnet transition temperature $T_N = 158$ K (Tables I and II). For these crystals there is no significant change in the lattice parameters or the volume upon cooling or warming through the magnetic transition, unlike pure $Fe_2P$ [1] and many

TABLE I. 230 K structural parameters for $FeMnP_{0.8}Si_{0.2}$—space group $P\bar{6}2m$ (189).

| | | | Atom coordinates | | | |
|---|---|---|---|---|---|---|
| Lattice constants | Site | Wycoff position | $x$ | $y$ | $z$ | Occ. f. |
| $a = b = 5.9681(38)$ Å | Fe(1) | $3f$ | 0.2539(2) | 0 | 0 | 1.000 |
| $c = 3.4966(22)$ Å | Mn(2) | $3g$ | 0.5900(3) | 0 | $\frac{1}{2}$ | 1.000 |
| $\alpha = \beta = 90°, \gamma = 120°$ | P(1) | $2c$ | $\frac{1}{3}$ | $\frac{2}{3}$ | 0 | 0.807 |
| | Si(1) | $2c$ | $\frac{1}{3}$ | $\frac{2}{3}$ | 0 | 0.193 |
| | P(2) | $1b$ | 0 | 0 | $\frac{1}{2}$ | 0.807 |
| | Si(2) | $1b$ | 0 | 0 | $\frac{1}{2}$ | 0.193 |
| Reliability factors | | $R_1$ | $wR_2$ | $R_{int}$ | GooF | |
| | | 0.0348 | 0.0658 | 0.0581 | 1.091 | |

TABLE II. 110 K structural parameters for $FeMnP_{0.8}Si_{0.2}$—space group $P\bar{6}2m$.

| Lattice constants | Site | Wycoff position | Atom coordinates $x$ | $y$ | $z$ | Occ. f. |
|---|---|---|---|---|---|---|
| $a = b = 5.9638(43)$ Å | Fe(1) | $3f$ | 0.2542(3) | 0 | 0 | 1.000 |
| $c = 3.4903(25)$ Å | Mn(2) | $3g$ | 0.5900(4) | 0 | $\frac{1}{2}$ | 1.000 |
| $\alpha = \beta = 90°, \gamma = 120°$ | P(1) | $2c$ | $\frac{1}{3}$ | $\frac{2}{3}$ | 0 | 0.807 |
| | Si(1) | $2c$ | $\frac{1}{3}$ | $\frac{2}{3}$ | 0 | 0.193 |
| | P(2) | $1b$ | 0 | 0 | $\frac{1}{2}$ | 0.807 |
| | Si(2) | $1b$ | 0 | 0 | $\frac{1}{2}$ | 0.193 |
| Reliability factors | $R_1$ | $wR_2$ | $R_{int}$ | GooF | | |
| | 0.0307 | 0.1078 | 0.0691 | 1.139 | | |

of the similar ferromagnetic magnetocaloric compositions (e.g., $FeMnP_{0.67}Si_{0.33}$) [27].

The magnetic properties of the crystals are shown in Figs. 2–4. The susceptibility data, taken with an applied field of 1 T (Fig. 2), indicate a magnetic transition at $T_N \approx 158$ K. Heating or cooling through the magnetic transition at 2 K/min results in about 1 K of hysteresis, which is small relative to many of the ferromagnetic compositions [1,13,19,20]. The magnetization curves ($M$ versus $H$) are linear at all temperatures (Fig. 4) with no evidence of a ferromagnetic intercept. Taken together Figs. 2 and 4 indicate antiferromagnetic order below 158 K with the spins oriented primarily in the $ab$ plane [28]. The magnetically ordered state is not simple, however, as is evident from the magnetic susceptibility, $\chi$, data above $T_N$ (Fig. 3). Above $T_N$, there is a maximum in the susceptibility at 295 K. From 400 to 700 K the decrease in $\chi$ is linear in $T(\chi = 7.8 \times 10^{-5} - 5.96 \times 10^{-8}\,\mathrm{T\,cm^3/g})$, with no evidence of Curie-Weiss behavior. Qualitatively similar results were obtained for $Fe_2P$ crystals [6]. For $Fe_2P$, neutron scattering data indicated substantial short-range order up to $T = 3T_c \approx 654$ K. Only above 700 K was Curie-Weiss behavior recovered [6].

Recent studies of polycrystalline samples with a nominal composition of $FeMnP_{0.75}Si_{0.25}$ found that the magnetic behavior was very different depending on whether the samples were quenched or slow cooled [21,29–31]. The quenched samples exhibited ferromagnetism and strong hysteresis with a Curie temperature near 250 K, while samples cooled more slowly showed an antiferromagnetic component with a Néel temperature near 150 K and very little hysteresis. Based on Mossbauer, magnetization, and crystallographic data and theory these authors concluded that the magnetic ground state depended on the degree of Fe/Mn cation order [29]. Complete occupancy of the $3g$ site with Mn favored antiferromagnetic order. Although the polycrystalline samples had small amounts of other impurity phases [29,31], and even the "purest" phases

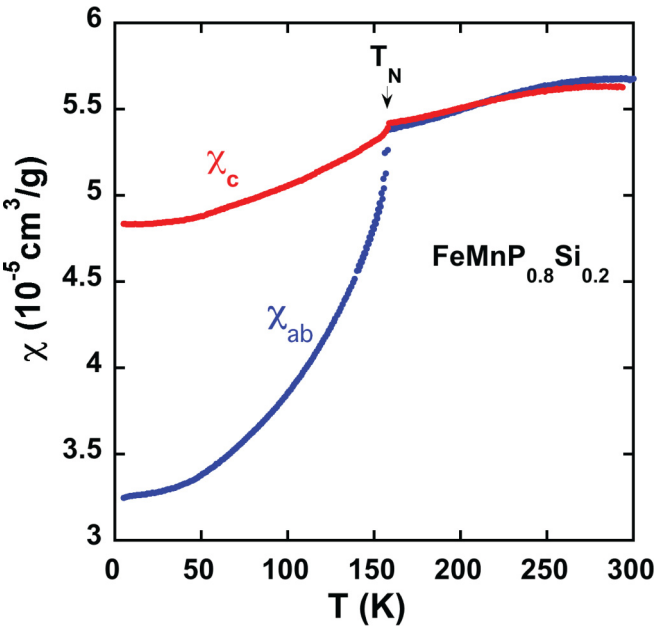


FIG. 2. (Color online) Magnetic susceptibility versus temperature for a $FeMnP_{0.8}Si_{0.2}$ single crystal with an applied magnetic field of $\mu_0 H = 1$ T applied parallel or perpendicular to the $\boldsymbol{c}$ axis. The susceptibility data indicate antiferromagnetic order with the spins oriented primarily in the $ab$ plane.

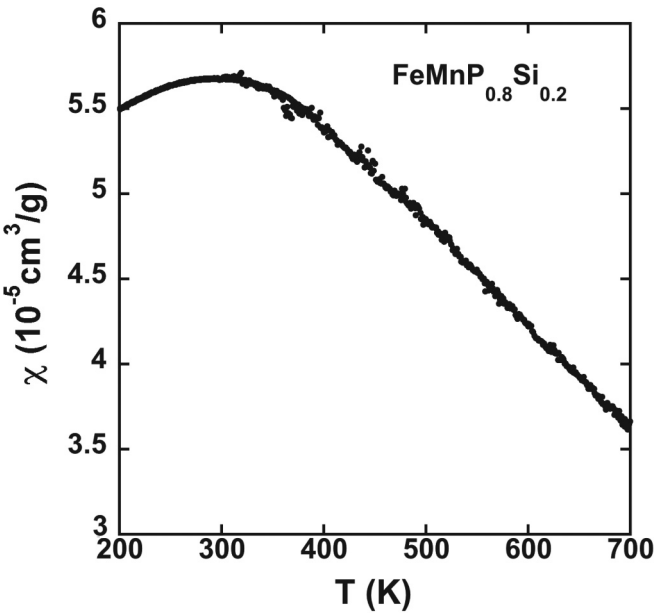


FIG. 3. Magnetic susceptibility versus temperature above $T_N \approx 158$ K with an applied magnetic field of $\mu_0 H = 1$ T. Between 400 and 700 K the decrease in $\chi(T)$ is linear, which is unusual and indicates complex magnetic behavior.

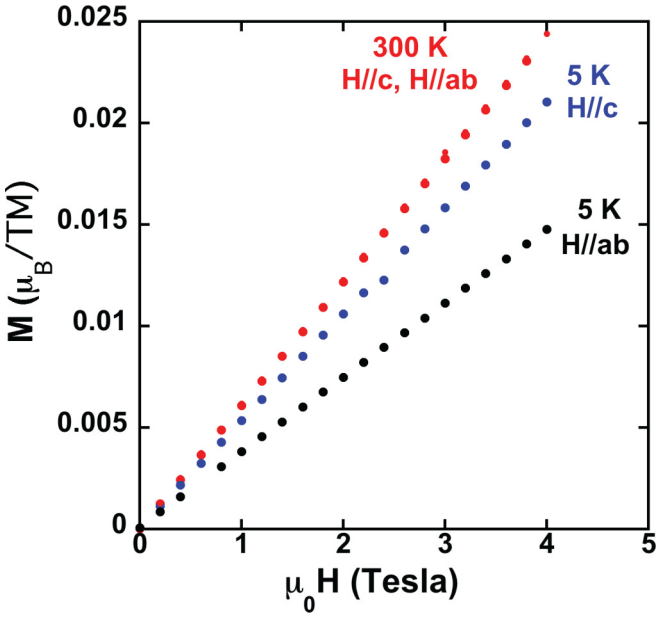


FIG. 4. (Color online) Magnetization versus magnetic field. No evidence of ferromagnetism is observed. The units of magnetization are given as the number of Bohr magnetons per transition metal atom.

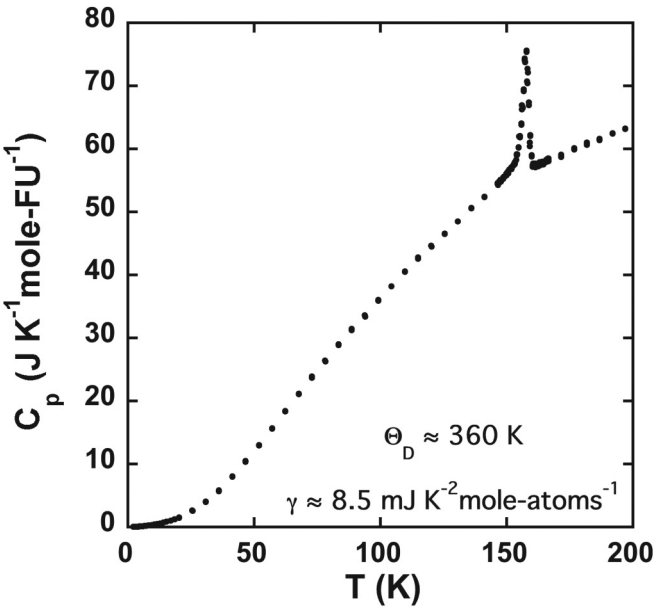


FIG. 5. Heat capacity versus temperature at $\mu_0 H = 0$. Heat capacity data taken with an applied magnetic field of $\mu_0 H = 8\,\mathrm{T}$ applied perpendicular to the ***c*** axis was the same as the 0 field data within experimental error.

had a mixture of ferromagnetic and antiferromagnetic order, the itinerant antiferromagnetic state is likely the same we observe in single crystals of $FeMnP_{0.8}Si_{0.2}$. Powder neutron diffraction from polycrystalline samples with a significant fraction of the antiferromagnetic phase indicated that the antiferromagnetism is incommensurate, with a wave vector $q_x = 0.361$. The proposed magnetic structure [31] is noncollinear with the spins lying in the *ab* plane. This magnetic structure is consistent with our single-crystal magnetic susceptibility data (Fig. 2) and the heat capacity data as discussed below.

Motivated by the very recent polycrystalline studies [29–31] on nominal $FeMnP_{0.75}Si_{25}$, single crystals of $FeMnP_{0.8}Si_{0.2}$ were wrapped in Ta foil to reduce oxidation, sealed under vacuum in a silica tube, and then heated to 1060 °C for 16 h followed by a rapid quench into water. For the quenched crystals no hint of ferromagnetism is observed in $M$ vs $H$ measurements at 5 K, but the Néel temperature was lowered slightly to about 152 K. These results suggest that the ordered arrangement of the Mn and Fe cations is likely the thermodynamically stable configuration for this composition.

Heat capacity data from the same crystal used for the magnetic measurements are shown in Figs. 5 and 6. In the temperature range from 2 to 200 K, the only phase transition evident is the magnetic transition at $T_N \approx 158\,\mathrm{K}$. The shape and magnitude of the heat capacity peak are similar to that observed in other materials that exhibit a spin-density wave transition (SDW) associated with an itinerant magnetic state [32,33]. The entropy associated with the transition at 158 K is estimated to be $\Delta S \approx 0.21\,\mathrm{J/K}$ per mole transition metal, which is only about 3% of Rln2, where R is the gas constant. The small entropy change is consistent with an itinerant antiferromagnet, although it is also likely that much of the entropy in the spin system is removed at higher temperatures due to short-range magnetic order. A standard Debye fit of the low-temperature heat capacity ($T < 8\,\mathrm{K}$) to $C_p \approx \gamma T + \beta T^3$ yields $\gamma = 8.5\,\mathrm{mJ/K^2}$ mole atoms, and a Debye temperature of $\Theta_D = 360\,\mathrm{K}$. This assumes that the magnetic contribution to $C_p$ below 8 K can be neglected. These values are similar to those reported for $Fe_2P$ of $8\,\mathrm{mJ/K^2}$ moleatoms and $\Theta_D = 420\,\mathrm{K}$ [34]. The heat capacity was also measured with a magnetic field of $\mu_0 H = 8\,\mathrm{T}$ applied perpendicular to the $c$ axis. Within experimental error there is no difference between the $\mu_0 H = 0$ and $\mu_0 H = 8\,\mathrm{T}$ heat capacity data. This is in

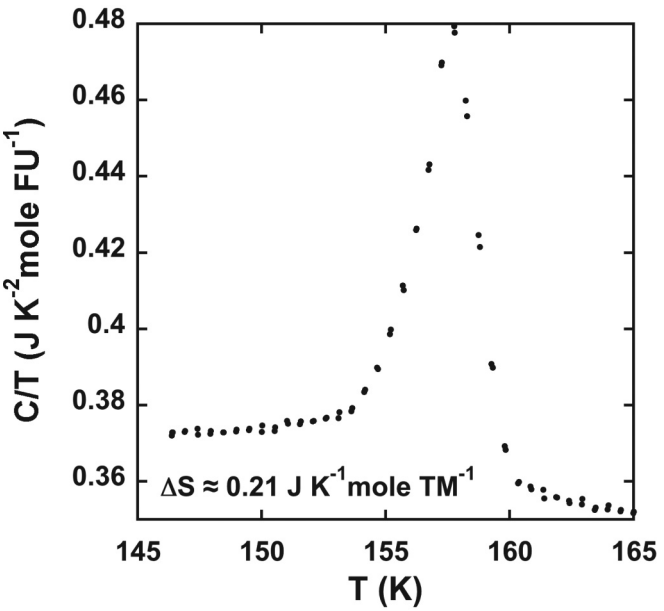


FIG. 6. Heat capacity divided by $T$ versus $T$ near the Néel temperature at $H = 0\,\mathrm{T}$. No significant change in the data is observed for $\mu_0 H = 8\,\mathrm{T}$. The entropy change is about 3.6% of Rln(2) per mole of transition metal.

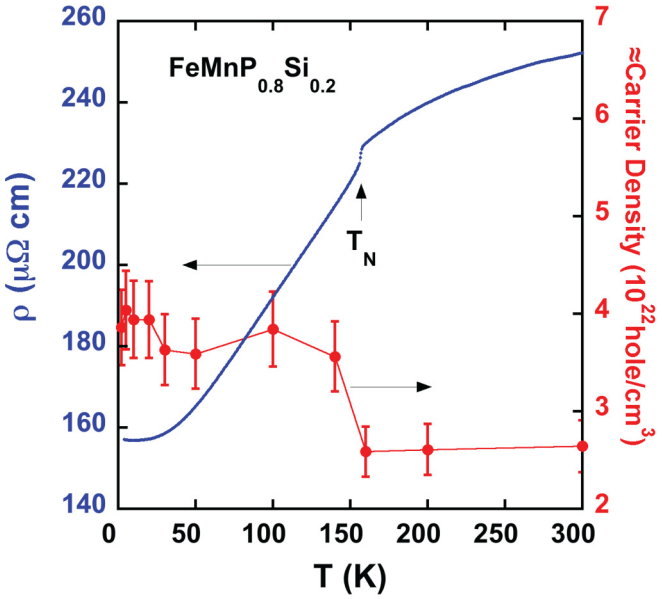


FIG. 7. (Color online) Resistivity versus temperature with $I//c$ (left axis) Apparent carrier concentration versus temperature (right axis).

marked contrast to the effects of a magnetic field on the heat capacity of $Fe_2P$ crystals [35].

Resistivity data, $\rho_c$, from a thinned crystal plate ($\approx 0.045 \times 0.35 \times 3$ mm) are shown in Fig. 7 with the current along the $c$ axis. The resistivity is weakly temperature dependent, but metallic at all temperatures. The magnitude of the resistivity is relatively high for a normal metal, but is typical for a semimetal or a heavily doped semiconductor. The sharp drop in the resistivity below $T_N$ is seen in most magnetic systems and is normally attributed to less magnetic scattering of the carriers in the magnetically ordered state. The magnitude of $\rho_c$ at 300 K is similar to that reported for a $Fe_2P$ crystal ($\approx 300\,\mu\Omega$ cm) [1]. For temperatures below $T_N$, however, the decrease in $\rho_c$ is only about 40%, presumably because of the added chemical disorder relative to pure $Fe_2P$. The apparent carrier concentration, $n_{app}$, is determined from the Hall coefficient, $R_H$, using a simple one band model ($R_H \approx 1/ne$). This is plausible since all of the Hall resistivity data are linear in magnetic field up to at least 6 T (not shown). Above $T_N$ the dominant carriers are holes and $n_{app} \approx 2.6 \times 10^{22}$ holes/cm$^3$. Just below $T_N$ there is an abrupt increase in $n_{app}$, followed by a more gradual net increase in $n_{app}$ down to 2 K. This behavior is unexpected since for most itinerant antiferromagnets part of the Fermi surface develops a gap below $T_N$, which should result in fewer carriers, not more. An apparent increase in the density of states below a magnetic transition is nonintuitive. One possible explanation for the Hall data below $T_N$ is that it is related to the anomalous Hall effect (AHE) often seen in ferromagnets [36]. The increase in $n_{app}$ below $T_N$ looks roughly like the temperature dependence of the local staggered magnetization in an antiferromagnet, but further research is needed to test this hypothesis. The transverse magnetoresistance is small at all temperatures ($\approx 0.04\%$ at 6 T), but is negative above $T_N$ and positive below (not shown). A positive magnetoresistance is normal for a metal, and the negative magnetoresistance above $T_N$ is normally associated with the proximity to ferromagnetism [37]. For $FeMnP_{0.8}Si_{0.2}$, the change in sign of the magnetoresistance at $T_N$ is at least an indicator of a change in the electronic structure at $T_N$.

As noted above, a room-temperature resistivity of $250\,\mu\Omega$ cm is large for a metallic system, and may be close to the Ioffe-Regel limit, $\rho_{sat}$, where the mean free path of the carriers approaches the interatomic distance, $a$ [38]. A simple model was proposed by Gurvitch [38] for $\rho_{sat} = 1.29 \times 10^{18}/n^{2/3}a\,\mu\Omega$ cm, where $n$ is the carrier concentration per cm$^3$, and the interatomic distance, $a$, is in angstroms. At room temperature using a value of $a = 3$ Å this gives a value of $\rho_{sat}$ of $490\,\mu\Omega$ cm for $FeMnP_{0.8}Si_{0.2}$, which is within a factor of 2 of the measured value at room temperature. The tendency of the resistivity to saturate at higher temperatures may reflect an approach to the Ioffe-Regel limit. We note that the data previously reported for the high-temperature resistivity of $Fe_2P$ single crystals show very little temperature dependence above 300 K [1].

## IV. SUMMARY AND CONCLUSIONS

In summary, millimeter-sized single crystals of $FeMnP_{0.8}Si_{0.2}$ are grown from a Sn flux. These are sizable single crystals grown with compositions close to those proposed for magnetocaloric applications [20,21]. The crystals are characterized with a variety of techniques including single-crystal x-ray diffraction, magnetization, magnetic susceptibility, heat capacity, Hall effect, and resistivity. Single-crystal x-ray diffraction indicates a strong preference for Mn to occupy the larger pyramidal $3g$ site in the $Fe_2P$ structure. The crystals are antiferromagnetic below $T_N \approx 158$ K with the spins oriented primarily in the $ab$ plane. Unlike many of the ferromagnetic magnetocaloric compositions [20], the antiferromagnetic transition is very weakly first order with only about 1 K hysteresis with heating and cooling rates of 2 K/ min. From heat capacity data, the change in magnetic entropy near $T_N$ is rather small (about 3% of Rln2), which suggests that the magnetic transition is of an itinerant SDW type. This is supported also by very recent powder neutron diffraction from an impure polycrystalline sample with a significant fraction of this antiferromagnetic phase. The antiferromagnetic phase was found to be incommensurate with a wave vector $q_x = 0.361$ [31]. Single-crystal magnetic susceptibility data above room temperature also suggest significant magnetic short-range order similar to what is observed in pure $Fe_2P$ [6]. Based on Hall data above $T_N$, the magnitude of the resistivity of $FeMnP_{0.8}Si_{0.2}$ (and likely that of $Fe_2P$) approaches the Ioffe-Regel limit for a metal. Below $T_N$, the increase in the apparent carrier concentration may be related to an anomalous Hall effect [39].

## ACKNOWLEDGMENTS

This work was supported by the U.S. Department of Energy, Office of Science, Basic Energy Sciences, Materials Sciences and Engineering Division. B.S.C. acknowledges support from the Critical Materials Institute, an Energy Innovation Hub, funded by the U.S. Department of Energy, Office of Energy Efficiency and Renewable Energy, Advanced Manufacturing Office.

[1] H. Fujii, T. Hokabe, T. Kamigaichi, and T. Okamoto, J. Phys. Soc. Jpn. **43**, 41 (1977).
[2] H. Fujii, T. Hokabe, H. Fujiwara, and T. Okamoto, J. Phys. Soc. Jpn. **44**, 96 (1978).
[3] H. Fujii, T. Hokabe, K. Eguchi, H. Fujiwara, and T. Okamoto, J. Phys. Soc. Jpn. **51**, 414 (1982).
[4] B. Carlsson, M. Golin, and S. Rundqvist, J. Solid State Chem. **8**, 57 (1973).
[5] R. Fruchart, A. Roger, and J. P. Senateur, J. Appl. Phys. **40**, 1250 (1969).
[6] H. Fujii, Y. Uwatoko, K. Motoya, Y. Ito, and T. Okamoto, J. Phys. Soc. Jpn. **57**, 2143 (1988).
[7] O. Eriksson, J. Sjoestroem, B. Johansson, L. Haeggstroem, and H. L. Skriver, J. Magn. Magn. Mater. **74**, 347 (1988).
[8] T. Moriya, J. Phys. Soc. Jpn. **51**, 420 (1982).
[9] H. Fujii, S. Komura, T. Takeda, T. Okamoto, Y. Ito, and J. Akimitsu, J. Phys. Soc. Jpn. **46**, 1616 (1979).
[10] H. Kadomatsu, M. Isoda, K. Tohma, H. Fujii, T. Okamoto, and H. Fujiwara, J. Phys. Soc. Jpn. **54**, 2690 (1985).
[11] P. Jernberg, A. A. Yousif, L. Haeggstroem, and Y. Andersson, J. Solid State Chem. **53**, 313 (1984).
[12] R. Chandra, S. Bjarman, T. Ericsson, L. Haeggstroem, C. Wilkinson, R. Waeppling, Y. Andersson, and S. Rundqvist, J. Solid State Chem. **34**, 389 (1980).
[13] N. H. Dung, Z. Q. Ou, L. Caron, L. Zhang, D. T. C. Thanh, G. A. de Wijs, R. A. de Groot, H. J. Buschow, and E. Brueck, Adv. Energy Mater. **1**, 1215 (2011).
[14] X. Z. Yu, Y. Onose, N. Kanazawa, J. H. Park, J. H. Han, Y. Matsui, N. Nagaosa, and Y. Tokura, Nature **465**, 901 (2010).
[15] F. Jonietz, S. Muehlbauer, C. Pfleiderer, A. Neubauer, W. Muenzer, A. Bauer, T. Adams, R. Georgii, P. Boeni, R. A. Duine, K. Everschor, M. Garst, and A. Rosch, Science **330**, 1648 (2010).
[16] I. E. Dzyaloshinsky, Phys. Chem. Solids **4**, 241 (1958).
[17] T. Moriya, Phys. Rev. **120**, 91 (1960).
[18] K. A. Gschneidner, Jr., V. K. Pecharsky, and A. O. Tsokol, Rep. Prog. Phys. **68**, 1479 (2005).
[19] O. Tegus, E. Brick, K. H. J. Buschow, and F. R. de Boer, Nature **415**, 150 (2002).
[20] F. Guillou, G. Porcari, H. Yibole, N. van Dijk, and E. Brueck, Adv. Mater. **26**, 2671 (2014).
[21] V. Hoeglin, J. Cedervall, M. S. Andersson, T. Sarkar, M. Hudl, P. Nordblad, Y. Andersson, and M. Sahlberg, RSC Adv. **5**, 8278 (2015)
[22] D. T. C. Thanh, E. Brueck, N. T. Trung, J. C. P. Klaasse, K. H. J. Buschow, Z. Q. Ou, O. Tegus, and L. Caron, J. Appl. Phys. **103**, 07B318 (2008).
[23] M. J. Neish, M. P. Oxley, J. Guo, B. C. Sales, L. J. Allen, and M. F. Chisholm, Phys. Rev. Lett. **114**, 106101 (2015).
[24] H. Okamoto, *Phase Diagrams for Binary Alloys*, 2nd ed. (ASM International, Materials Park, OH, 2010).
[25] N. E. Alekseevskii and Y. P. Gaidukov, Zh. Eksp. Teor. Fiz. **36**, 447 (1959).
[26] B. C. Sales, R. Jin, and D. Mandrus, Phys. Rev. B **77**, 024409 (2008).
[27] F. Guillou, H. Yibole, N. H. van Dijk, and E. Brueck, J. Alloys Compd. **632**, 717 (2015).
[28] S. Blundell, *Magnetism in Condensed Matter* (Oxford University Press, New York, 2001).
[29] M. Hudl, P. Nordblad, T. Bjorkman, O. Eriksson, L. Haggstrom, M. Sahlberg, Y. Andersson, E.-K. Delczeg-Czirjak, and L. Vitos, Phys. Rev. B **83**, 134420 (2011).
[30] E. K. Delczeg-Czirjak, L. Bergqvist, O. Eriksson, Z. Gercsi, P. Nordblad, L. Szunyogh, B. Johansson, and L. Vitos, Phys. Rev. B **86**, 045126 (2012).
[31] V. Hoeglin, M. Hudl, L. Caron, P. Beran, M. H. Soerby, P. Nordblad, Y. Andersson, and M. Sahlberg, J. Solid State Chem. **221**, 240 (2015).
[32] B. C. Sales, R. Jin, K. A. Affholter, P. Khalifah, G. M. Veith, and D. Mandrus, Phys. Rev. B **70**, 174419 (2004).
[33] G. Gruner, Rev. Mod. Phys. **66**, 1 (1994).
[34] O. Beckman, L. Lundgren, P. Nordblad, P. Svedlindh, A. Toerne, Y. Andersson, and S. Rundqvist, Phys. Scr. **25**, 679 (1982).
[35] M. Hudl, D. Campanini, L. Caron, V. Hoglin, M. Sahlberg, P. Nordblad, and A. Rydh, Phys. Rev. B **90**, 144432 (2014).
[36] B. C. Sales, R. Jin, D. Mandrus, and P. Khalifah, Phys. Rev. B **73**, 224435 (2006).
[37] A. B. Pippard, *Magnetoresistance in Metals* (Cambridge University Press, Cambridge, 1989).
[38] M. Gurvitch, Phys. Rev. B **24**, 7404 (1981).
[39] H. Chen, Q. Niu, and A. H. MacDonald, Phys. Rev. Lett. **112**, 017205 (2014).